



**HAL**  
open science

## The impact of oxidation on the optical properties of Si–SiC materials

Ludovic Charpentier, Cyril Caliot, Jean-Louis Sans, Angélique Bousquet

► **To cite this version:**

Ludovic Charpentier, Cyril Caliot, Jean-Louis Sans, Angélique Bousquet. The impact of oxidation on the optical properties of Si–SiC materials. *Ceramics International*, 2020, 46, pp.28536. 10.1016/j.ceramint.2020.08.011 . hal-02916030

**HAL Id: hal-02916030**

**<https://hal.science/hal-02916030v1>**

Submitted on 17 Aug 2020

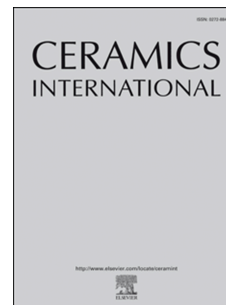
**HAL** is a multi-disciplinary open access archive for the deposit and dissemination of scientific research documents, whether they are published or not. The documents may come from teaching and research institutions in France or abroad, or from public or private research centers.

L'archive ouverte pluridisciplinaire **HAL**, est destinée au dépôt et à la diffusion de documents scientifiques de niveau recherche, publiés ou non, émanant des établissements d'enseignement et de recherche français ou étrangers, des laboratoires publics ou privés.

# Journal Pre-proof

The impact of oxidation on the optical properties of Si–SiC materials

Ludovic Charpentier, Cyril Caliot, Jean-Louis Sans, Angélique Bousquet



PII: S0272-8842(20)32376-2

DOI: <https://doi.org/10.1016/j.ceramint.2020.08.011>

Reference: CERI 26113

To appear in: *Ceramics International*

Received Date: 10 April 2020

Revised Date: 15 July 2020

Accepted Date: 3 August 2020

Please cite this article as: L. Charpentier, C. Caliot, J.-L. Sans, Angé. Bousquet, The impact of oxidation on the optical properties of Si–SiC materials, *Ceramics International* (2020), doi: <https://doi.org/10.1016/j.ceramint.2020.08.011>.

This is a PDF file of an article that has undergone enhancements after acceptance, such as the addition of a cover page and metadata, and formatting for readability, but it is not yet the definitive version of record. This version will undergo additional copyediting, typesetting and review before it is published in its final form, but we are providing this version to give early visibility of the article. Please note that, during the production process, errors may be discovered which could affect the content, and all legal disclaimers that apply to the journal pertain.

© 2020 Published by Elsevier Ltd.

# The impact of oxidation on the optical properties of Si-SiC materials

Ludovic Charpentier<sup>\*,a</sup>, Cyril Caliot<sup>a</sup>, Jean-Louis Sans<sup>a</sup>, Angélique Bousquet<sup>b</sup>

<sup>a</sup> Laboratoire PROcédés, Matériaux et Energie Solaire, PROMES-CNRS, 7 rue du Four Solaire  
66120 Font-Romeu Odeillo, France

<sup>b</sup> Université Clermont Auvergne/CNRS, Institut de Chimie de Clermont-Ferrand, 24 avenue  
Blaise Pascal, 63178 Aubière, France

**Abstract.** Silicon carbide is an interesting candidate for high-temperature solar receiver due to its high solar absorptivity and its resistance to oxidation in air. Its oxidation stays passive with the formation of a protective silica layer up to 1900 K. Nevertheless, silica presents a lower spectral emissivity than silicon carbide in the solar range. Therefore the growth of a silica layer may affect the values of the spectral emissivity and therefore the surface receiver thermal efficiency. We have investigated here how high-temperature ageing in air affects the spectral emissivity and the thermal efficiency of commercial Si-SiC materials. We were able to correlate the variations of the spectral emissivities to the advancement of the oxidation using scanning electron microscopy, ellipsometry and 3D profilometry. Especially we observed a significant improvement of the surface receiver thermal efficiency due to the increase of the surface roughness that increases the solar absorptivity.

**Keywords.** D-SiC; C-Corrosion; C-Optical properties; E-Heat exchangers

## 1. Introduction

The future generation of solar power plants (SPP) will use solar tower technology that requires high temperature and high solar concentrated power at the receiver [1]. Receiver

---

\* Corresponding author, Ludovic.Charpentier@promes.cnrs.fr

materials will therefore be subject to strong thermo-mechanical constraints caused by rapid temperature increases and decreases during transitory operation as well as thermal gradients during normal operation [2]. In addition, at high temperature, the thermal emission of the receiver toward the environment dominates the thermal losses [3]. To limit these losses, selective materials presenting a high solar absorptivity and a low infrared (IR) emissivity should be used [4]. Finally, the irradiated surface of the receiver may be exposed directly to air (open-air receiver) preventing the use of a window that would reflect part of the concentrated solar flux and increase the receiver manufacturing complexity and its price.

A numerical study about the influence of the wall material optical properties of high temperature solar receivers was reported by Larrouturou *et al.* [4] and quantifies the improvement of the solar-to-electric efficiency of an SPP obtained by using selective materials, such as tantalum carbide (TaC). Nevertheless we have recently observed that TaC presents a really poor resistance towards oxidation, and once oxidized, this material shows a “reverse selectivity”: the oxidized material has a solar absorptivity lower than its IR emissivity. So TaC can be excluded from the open-air solar receiver [5].

SiC does not present a spectral selectivity as strong as the one of TaC [6], but it can form silica up to 1900 K in air at atmospheric pressure [7]. In this passive oxidation regime, the oxidation kinetics tends to become semi-parabolic, this kinetics being controlled by the molecular diffusion of oxide through the produced oxide layer according to the Deal and Grove model [8]. So limited damages in operating conditions are expected with this material. In a recent work, the total hemispherical emissivity of sintered SiC was measured in air and high vacuum at temperatures up to 1850 K using a direct method [9]. The main conclusion was that the influence of the *in situ* grown oxide layer on the emissivity depends on its

thickness: the emissivity decreases when the thickness of the oxide layer increases up to 120 nm, then it increases with the thickness for thicker oxides due to the huge increase of the surface roughness.

We are continuing this approach in this work, investigating how a longer ageing of a commercial Si-SiC material may affect its spectral emissivity. The measurement of the spectral emissivity (and not the total emissivity as previously done [9]) will enable us to separate the influence of the oxidation on the solar absorptivity and on the IR emissivity. And therefore to determine how the thermal efficiency of one surface receiver would be affected by the advancement of the oxidation.

## **2. Materials and methods**

### **2.1 Materials**

The Si-SiC materials were purchased to the EngiCer SA company [10]. The Si content is 10 v. %. Some impurities such as Al are present at content below 0.2 v. % Pellets of 25 mm-diameter and 2mm-thickness were obtained using hot-pressing at 1750 K.

Figure 1 is presenting the SEM imaging (in secondary electron – SE – mode) of the reference samples. The phases were identified by EDS (figure 2). We observed the presence of large Si grains ( $\approx 5\mu\text{m}$  of characteristic length) at the surface surrounded by smaller SiC grains, so we supposed there was a migration of liquid silicon to the surfaces during the hot pressing.

### **2.2 High temperature oxidations**

The high temperature oxidations of the Si-SiC samples were performed using the REHPTS (*RÉacteur Hautes Pression et Température Solaire* – High Pressure and Temperature Solar Reactor). This reactor is based at the focus of a 6kW solar furnace. The upper surface of the

Si-SiC samples was insulated and the temperature was homogeneous on a 10 cm-diameter surface. A shutter enables to control the fraction of the concentrated solar flux irradiating the sample, therefore controlling the sample surface temperature that is measured at the center of it (on a 6 mm-diameter area), using a monochromatic optical pyrometer (at  $\lambda = 5\mu\text{m}$ ) Iacon Modline. The atmosphere inside REHPTS was open to air at  $P = 87 \text{ kPa}$  (this pressure is the atmospheric one at the altitude of the solar furnace, 1500 m). More details on this facility and its equipment have been previously published [11, 12]. The samples were heated in a few seconds up to the desired temperature, then kept during 20 minutes or one hour at this temperature, and cooled down to room temperature. The mass variation was obtained by weighting the samples (the balance precision is  $\pm 0.1 \text{ mg}$ ) before and after each oxidation, 4 cycles of oxidation being performed. Table 1 summarizes the operating conditions for each sample.

Reference of the sample	Oxidation durations (number of cycle x duration of each cycle)	Temperature (K)
SiSiC_4	4 x 20 min.	1470
SiSiC_5	4 x 20 min.	1530
SiSiC_6	4 x 1 h.	1500

**Table 1.** Operating conditions for the samples oxidized inside REHPTS.

## 2.3 Emissivity measurements

### 2.3.1 Room temperature measurements

The Perkin Elmer lambda 950 and the SOC 100 HDR set-ups were used to measure the reflectivity of the Si-SiC samples at room temperature (300 K). The first set-up measures

normal hemispherical reflectivity in a spectral range from 250 to 2500 nm, the second one enables the determination of the hemispherical directional reflectance in the interval from 2 to 25  $\mu\text{m}$ . These set-ups can also measure the transmittance, so we used them to check the opacity of the samples and in such case, the room temperature normal spectral emissivity  $\varepsilon(\lambda)$  can be obtained from eq. (1). The hypothesis is made that the Kirchhoff's law of thermal radiation applies and therefore the spectral absorptivity is considered equal to the spectral emissivity. The room temperature solar absorptivity  $\alpha$  and the total emissivity  $\varepsilon$  can be deduced from eq. (2) and (3), respectively.

$$\varepsilon(\lambda) = 1 - \rho(\lambda) - \tau(\lambda) \quad (1)$$

$$\alpha = \frac{\int_{0.25}^{2.5} \varepsilon(\lambda) \cdot I(\lambda) d\lambda}{\int_{0.25}^{2.5} I(\lambda) d\lambda} \quad (2)$$

$$\varepsilon = \frac{\int_{0.25}^{25} \varepsilon(\lambda) \cdot E^{bb}(\lambda, 300 \text{ K}) d\lambda}{\int_{0.25}^{25} E^{bb}(\lambda, 300 \text{ K}) d\lambda} \quad (3)$$

Tabulations of the incoming solar irradiance  $I(\lambda)$  can be found online, we used the Reference Air Mass 1.5 Spectra from the National Renewable Energy Laboratory [13]. The blackbody emittance at 300 K  $E^{bb}(\lambda, 300 \text{ K})$  was calculated using the Planck's law.

### 2.3.2 High temperature measurements

High temperature radiative measurements were performed using solar concentrated radiation. The samples placed inside the MEDIASE (*Moyen d'Essais et Diagnostic en Ambiance Spatiale Extreme*) facility at the focus of the 1 MW solar furnace and previously described [14-16] were heated on one face with concentrated solar radiation and a CI Systems SR-5000N spectroradiometer measured the normal spectral emissivity on the other side in a spectral range from 1.4 to 14  $\mu\text{m}$  in the 1100-1600 K interval. These measurements

were integrated over two spectral intervals, 1.4-2.8  $\mu\text{m}$  and 1.4-14  $\mu\text{m}$ , according to equation (4) and (5):

$$\varepsilon_{1.4-2.8}(T) = \frac{\int_{1.4}^{2.8} \varepsilon(\lambda, T) \cdot I(\lambda) \cdot d\lambda}{\int_{1.4}^{2.8} I(\lambda) \cdot d\lambda} \quad (4)$$

$$\varepsilon_{1.4-14}(T) = \frac{\int_{1.4}^{14} \varepsilon(\lambda, T) \cdot E_{bb}(\lambda, T) \cdot d\lambda}{\int_{1.4}^{14} E_{bb}(\lambda, T) \cdot d\lambda} \quad (5)$$

where  $I(\lambda)$  is the earlier described incoming solar irradiance and  $E_{bb}$  is the blackbody emittance calculated at  $T$ . The average emissivities given by equations (4) and (5) are approximate values of the solar absorptivity  $\alpha$  (if the Kirchhoff's law of thermal radiation applies) and of the total emissivity  $\varepsilon$ . A two-color pyro-reflectometer developed at PROMES-CNRS measured the actual surface temperature [17]. The pyro-reflectometer and the spectroradiometer were previously calibrated on a blackbody.

## 2.4 Post-experimental analyses

SEM imaging, coupled with Energy-dispersive x-ray spectroscopy (EDS), was performed using a Hitachi S-4500 apparatus. The surface roughness before and after oxidation was measured using a Leica DCM 3D optical profilometer according to a previously described procedure [5]. We used a magnification of 100x. Profilometry gave the variation of the height  $z$  as a function of the positions  $x$  and  $y$  on the surface of the sample. Five different surfaces (of length and width  $l = L = 0.5$  mm) were scanned on each reference and oxidized samples to obtain average values of the arithmetic and quadratic surface roughness  $S_a$  ( $\overline{\Delta z}$ ) and  $S_q$  ( $\sqrt{\overline{\Delta z^2}}$ ) and of the maximum deviation  $S_z$  ( $z_{max} - z_{min}$ ).

Finally, we performed ellipsometry with a Jobin-Yvon UVISSEL (0.75–4.75eV and fixed 70° incident angle) apparatus at the ICCF-CNRS laboratory according to a procedure previously



used on oxidized SiC [9]. The thickness of a semi-transparent oxide layer was estimated from a Tauc-Lorenz model [18, 19] commonly used to describe the dielectric function of insulator or semiconductor thin films. Two or three runs of measurements were performed on each sample, compared to measurements on a non-oxidized reference Si-SiC and on a reference SiO<sub>2</sub> layer.

### 3. Results and discussions

#### 3.1 Oxidation

Figure 3 presents the mass variation of the Si-SiC samples oxidized according to the operating conditions reported in table 1. A mass gain is observed, which is due to the formation of a SiO<sub>2</sub> layer that is heavier (60 g mol<sup>-1</sup>) than the consumed SiC (40 g mol<sup>-1</sup>) according to equation (6). The oxidation kinetics increases with the temperature. Nevertheless at 1470 K the mass variation is close to the balance precision. For the 4h-experiment at 1500 K, the oxidation rate slows down with time, with a weight variation close to the balance precision, which is coherent with the appearance of an expected diffusion-controlled regime [8].



Figure 4 presents the SEM images of the three oxidized samples. The growth of a blurred and non-conductive oxide layer is observed. Figure 5 presents the EDS spectra of the surfaces presented in figure 4. The presence of oxygen is clearly relevant from the growth of an oxide layer. The peak of aluminum is also appearing, probably due to the migration of the aluminum impurities to the surface during oxidation.

Figure 6 presents the evolution of the surface roughness with the oxidation. The arithmetic and quadratic roughness and the maximum deviation increase with the oxidation temperature and time.

Figure 7 a) presents the variations of the square of the mass variation  $(m-m_0)^2$  according to temperature. The fitting is improved at higher temperatures, as shown by regression coefficients higher than 0.9. Nevertheless, we could not perform experiments at temperatures higher than 1550 K due to the appearance of a liquid phase that is probably a Si(Al) liquid solution [20]. From the slope of the trend lines we can estimate the values of the semi-parabolic constant  $k_p$  as the oxidation regime is diffusion-controlled and figure 7 b) plots the values of  $k_p$  according to the reverse temperature  $1/T$ . The trend follows an Arrhenius law:

$$k_p = A \cdot \exp\left(-\frac{E_a}{RT}\right) \quad (6)$$

From the exponential coefficient given by figure 11 b) and according to equation (6), the activation energy  $E_a$  is estimated around  $820 \text{ kJ mol}^{-1}$ . This relatively high value of  $E_a$  can be explained by the presence of aluminum that enhances the oxygen diffusion through the silica layer [21].

### 3.2. Oxide thickness

Figure 8 presents the refractive index  $n$  and extinction coefficient  $k$ , obtained for the three oxidized samples, the Si-SiC reference sample and the reference  $\text{SiO}_2$  layer. The oxidation is indicated by a diminution of both parameters compared to the ones of non-oxidized Si-SiC. These parameters are also sometimes lower than the ones of  $\text{SiO}_2$ . Cross-section SEM images coupled with EDS cartography (figure 9) shows, as previously observed in figure 5,

the enrichment of the surface of the oxide layer in aluminum with the oxidation time whereas the Al distribution is homogeneous in the reference sample. This preferential oxidation of aluminum, even in residual amount, has been previously observed by several authors [22-25]. The oxide layer on sample Si-SiC 4 and 5 is too thin to be determined by SEM and EDS, even if a slight enrichment in oxygen and aluminum is observed at the surface whereas the thickness of the one on Si-SiC 6 is close to 2  $\mu\text{m}$ . Finally, table 2 reports the oxide thickness measured using ellipsometry data with two models according to two hypothesis:

- Hypothesis 1: the oxide layer is homogeneously made of semi-transparent material.
- Hypothesis 2: the oxide layer is constituted of one transparent layer and one modified layer with an oxygen exponential gradient.

As can be deduced from table 2, the second hypothesis gives results more coherent with the SEM observations regarding the Si-SiC 6 sample.

	<b>Hypothesis 1</b>	<b>Hypothesis 2</b>
Si-SiC 4	94-87	310-401
Si-SiC 5	94-88-87	417-413-361
Si-SiC 6	115-102	763-625

**Table 2.** Thickness of the oxide layers (nm) calculated from ellipsometry data according to the two hypotheses made.

The model related to the hypothesis of a bi-layered oxide gives thicknesses from 310 to 763 nm. The oxide layer grown on the Si-SiC 6 sample that was oxidized during 4 cycles of 1h at 1500 K is the thickest one. Its thickness ranges from 625 to 763 nm and is close to the order of the SEM/EDS estimation (2  $\mu\text{m}$ ). This overestimation is due to the fact the sample cross-

section may be tilted on one hand, and to the average width of the EDS/SEM pear on the other hand.

### 3.3 Measurement of radiative properties

Figure 10 presents the room temperature spectral emissivities in the 0.25-2.5  $\mu\text{m}$  (fig. 10 a) and 2-25  $\mu\text{m}$  (fig. 10 b) ranges, together with the values of solar absorptivity  $\alpha$  and total emissivity  $\varepsilon$  deduced from ed. (2) and (3) (fig. 10 c) and the  $\alpha/\varepsilon$  ratio (fig. 10 d). It is noticeable that the spectral emissivity of the oxidized sample increases in the 0.25-2  $\mu\text{m}$  range (fig. 10 a), which can be correlated to the increase of the surface roughness previously observed and decreases around 8  $\mu\text{m}$  (fig. 10 b), where is located a specific reflectivity peak for the silica [6]. Consequently a significant increase of the solar absorptivity (fig. 10 c) and of the  $\alpha/\varepsilon$  ratio (fig. 10 d) is observed.

High-temperature emissivity measurements were performed using MEDIASE in open air on the sample that was oxidized during 4x1h at 1500 K. Figure 11 presents the evolution with temperature of the spectral emissivity (fig. 11 a), of integrated  $\varepsilon_{1.4-2.8}$ ,  $\varepsilon_{1.4-14}$  and of the ratio between these two values (fig. 11 b). The emissivity drops at 2.7, 5.9 and 6.5  $\mu\text{m}$  on figure 8 a) are due to the absorption by surrounding  $\text{CO}_2$  and  $\text{H}_2\text{O}$  (the content of these absorbing gases is different in the measurement area from the calibration room), one located around 9  $\mu\text{m}$  corresponds to the silica, the last one around 12.5  $\mu\text{m}$  corresponds to the Si-C bond. The location of this minimum emissivity shifts with temperature towards higher wavelength, as already observed by previous authors although the cause of this shift is still not theoretically understood [26-27].  $\varepsilon_{1.4-2.8}$  stays nearly constant while the temperature increases from 1085 to 1490 K.  $\varepsilon_{1.4-14}$  slightly increases with the temperature, which can be due to the fact the maximum of the blackbody emittance spectrum shifts to lower wavelengths with higher spectral emissivity while the temperature increases. Consequently, a minor decrease of the ratio is observed from 1.14 at 1085 K to 1.11 at 1490 K.

The main changes in the room temperature optical properties and the high temperature radiative measurements are due to the growth of an oxide layer that provokes a significant spectral emissivity drop around  $8\mu\text{m}$ . An improvement of the room temperature spectral emissivity in the solar range is also observed, which is probably due to the higher roughness of the sample surface, as previously observed [5]. Consequently, an improvement of the room temperature  $\alpha/\varepsilon$  ratio is observed, from 1.2 to 1.4. At high temperature, a minor increase of the total emissivity (integrated on the 1.4 to  $14\mu\text{m}$  range) was observed, but this does not affect significantly the ratio with the approximate solar absorptivity (integrated on the 1.4 to  $2.8\mu\text{m}$  range), that stays around 1.1. The sample surface keeps on absorbing more solar concentrated energy that it may lose by radiative transfer to the outside, so the ratio stays correct.

Figure 12 presents computed values of the thermal efficiency  $\eta_R$  of a surface solar receiver (calculation is explained in reference [3]) with non-oxidized and oxidized Si-SiC (during  $4 \times 20$  min. at 1530 K) and with an incident solar flux  $P_i = 600\text{ kW m}^{-2}$  and an ambient temperature  $T_a = 300\text{ K}$ . The values of  $\alpha$  and  $\varepsilon$  used are the values on figure 10 c), *i.e.*  $\alpha = 0.83$  and  $0.9$ ,  $\varepsilon = 0.69$  and  $0.66$ , for reference and oxidized samples, respectively. This figure shows the oxidation could improve the thermal efficiency from 65 to 75% at 1200 K.

#### 4. Conclusion

The main feature in the oxidation of the commercial high temperature Si-SiC materials tested is the growth of a thin alumina layers due to the presence of residual Al impurities in the sample in lower amount than 0.2 v. %. This presence of aluminum enhances the semi-parabolic oxidation kinetics with activation energy of  $820\text{ kJ mol}^{-1}$ . Ellipsometry gave a satisfactory measurement of the thickness, once the presence of a bi-layered oxide was

taken into account. This thickness ranges from 310 to 763 nm. The growth of this oxide layer increases the solar absorptivity and makes the thermal emissivity decrease.

Future works will focus on the oxidation and thermal emissivities of pure SiC, in order not to get the contribution of Al impurities. Especially, the role of the thermal excitement in the displacement of the minimal value of the spectral emissivity corresponding to the Si-C bond with temperature is still to be understood.

## 5. Acknowledgements

This work was supported by the French program “investissement d’avenir” funded by the national research agency (France) under the codes ANR-10-LABX-22-01-SOLSTICE and ANR-10-EQPX-49-SOCRATE. The authors thank Christophe Escape from PROMES-CNRS for the room temperature optical measurements and Yonko Gorand from the University Perpignan Via Domitia for the SEM imaging and EDS spectra and mappings.

## 6. References

- [1] M. A. Silva-Pérez, Solar power towers using supercritical CO<sub>2</sub> and supercritical steam cycles, and decoupled combined cycles, in: M. J. Blanco, L. Ramirez Santigosa (Eds.), *Advances in Concentrating Solar Thermal Research and Technology*, Woodhead Publishing, Sawston, Cambridge, 2016, pp.383-402.
- [2] J. Capeillère, A. Toutant, G. Olalde, A. Boubault, Thermomechanical behavior of a plate ceramic solar receiver irradiated by concentrated sunlight, *Sol. Energy* 110 (2014) 174-187.
- [3] F. Larroutou, C. Caliot, G. Flamant, Effect of directional dependency of wall reflectivity and incident concentrated solar flux on the efficiency of a cavity solar receiver, *Sol. Energy* 109 (2014) 153-164.

- [4] F. Larroutourou, C. Caliot, G. Flamant, Influence of receiver surface spectral selectivity on the solar-to-electric efficiency of a solar tower power plant, *Sol. Energy* 130 (2016) 60–73.
- [5] L. Charpentier, C. Caliot, The impact of the oxidation on the optical properties of TaC, *Sol. Energ. Mat. Sol. C.* 171 (2017), 16-23.
- [6] Y.S. Touloukian, D.P. Dewitt, Thermophysical properties of matter - The TPRC Data Series - Vol. 8. Thermal radiative properties - Nonmetallic Solids, IFI/Plenum, New York-Washington, 1972.
- [7] W. L. Vaughn, H. G. Maas, Active-to-passive transition in the oxidation of silicon carbide and silicon nitride in air, *J. Am. Ceram. Soc.* 73 (1990) 1540-1543.
- [8] B. E. Deal, A. S. Grove, General relationship for the thermal oxidation of silicon, *J. Appl. Phys.* 36 (1965) 3770-3778.
- [9] M. Balat-Pichelin, A. Bousquet, Total hemispherical emissivity of sintered SiC up to 1850 K in high vacuum and in air at different pressures, *J. Eur. Ceram. Soc.* 38 (2018) 3447-3456.
- [10] EngiCer SA, Viale Pereda 22, 6828 Balerna, Switzerland. <http://www.engicer.com> (last access on April 2<sup>nd</sup>, 2020)
- [11] L. Charpentier, M. Balat-Pichelin, F. Audubert, High temperature oxidation of SiC under helium with low-pressure oxygen-part 1: sintered  $\alpha$ -SiC, *J. Eur. Ceram. Soc.* 30 (2010) 2653–2660.
- [12] L. Charpentier, M. Balat-Pichelin, J.-L. Sansa, D. Sciti, L. Silvestroni, Effect of high temperature oxidation on the radiative properties of HfC-based ceramics, *Corros. Sci.* 126 (2017) 255–264.
- [13] Reference Solar Spectral Irradiance: Air Mass 1.5, American Society for Testing and Materials (ASTM), USA. <http://rredc.nrel.gov/solar/spectra/am1.5/> (last access on April 2<sup>nd</sup>, 2020)
- [14] T. Paulmier, M. Balat-Pichelin, D. Le Quéau, R. Berjoan and J.F. Robert, Physico-chemical behavior of carbon materials under high temperature and ion irradiation, *Appl. Surf. Sci.* 180 (2001) 227-245.

- [15] M. Balat-Pichelin, J.F. Robert and J.L. Sans, Emissivity measurements on carbon-carbon composites at high temperature under high vacuum, *Appl. Surf. Sci.* 253 (2006) 778-783.
- [16] E. Brodu, M. Balat-Pichelin, J.L. Sans, M.D. Freeman and J.C. Kasper, Efficiency and behavior of textured high emissivity metallic coatings at high temperature, *Mater. Des.* 83 (2015) 85-94.
- [17] D. Hernandez, J.L. Sans, A. Netchaieff, P. Ridoux and V. Le Sant, Experimental validation of a pyroreflectometric method to determine the true temperature of an opaque surface without hampering reflections, *Measurement* 42 (2009) 836-843.
- [18] G.E.J. Jellison, F.A. Modine: Parameterization of the optical functions of amorphous materials in the interband region, *Appl. Phys. Lett.* 69 (1996) 371-373.
- [19] G.E.J. Jellison, V.I. Merkulov, A.A. Puretzky, D.B. Geohegan, G. Eres, D.H. Lowndes, J.B. Caughman, Characterization of thin-film amorphous semiconductors using spectroscopic ellipsometry, *Thin Solid Films* 377-378 (2000) 68-73.
- [20] L. García, C. Dietz, A. J. Criado, J. A. Martínez, Selective etching procedure for observation of primary silicon morphologies in V- $\text{AlSi}_2\text{O}$  master alloy, *Prakt. Metallogr.* 50 (2014) 709-721.
- [21] A. Kovalcikova, J. Sedlacek, Z. Lences, R. Bystricky, J. Dusza, P. Sajgalik, Oxidation resistance of SiC ceramics prepared by different processing routes, *J. Eur. Ceram. Soc.* 36 (2016) 3783-3793.
- [22] E. Opila, Influence of Alumina Reaction Tube Impurities on the Oxidation of Chemically-Vapor-Deposited Silicon Carbide, *J. Am. Ceram. Soc.* 78 (1995) 1107-1110.
- [23] K. Suzuki, N. Kageyama, T. Kanno, Improvement in the oxidation resistance of liquid-phase-sintered silicon carbide with aluminum oxide additions, *Ceram. Int.* 31 (2005) 879-882.
- [24] S.C. Singhal, F.F. Lange, Effect of Alumina Content on the Oxidation of Hot-Pressed Silicon Carbide, *J. Am. Ceram. Soc.* 58 (1975) 433-435.



- [25] L. Charpentier, A. Maître, M. Balat-Pichelin, S. Foucaud, F. Audubert, Influence of alumina on the passive oxidation at low oxygen pressure of hot-pressed  $\alpha$ -SiC, *Scripta Mater.* 60 (2009) 481–484.
- [26] C. P. Cagran, L. M. Hanssen, M. Noorma, A. V. Gura, S. N. Mekhontsev, Temperature-Resolved Infrared Spectral Emissivity of SiC and Pt–10Rh for Temperatures up to 900°C, *Int. J. Thermophys.* 28 (2007) 581-597.
- [27] F. Wang, L. Cheng, L. Xiang, Q. Zhang, L. Zhang, Effect of SiC coating and heat treatment on the thermal radiation properties of C/SiC composites, *J. Eur. Ceram. Soc.* 34 (2014) 1667-1672.

**List of table captions**

**Table 1.** Operating conditions for the samples oxidized inside REHPTS.

**Table 2.** Thickness of the oxide layers (nm) calculated from ellipsometry data according to the two hypothesis made.

Journal Pre-proof

### List of figure captions

**Figure 1.** SEM images at the center of the Si-SiC reference material (a) x 1,000 (b) x 6,000

**Figure 2.** EDS spectrum on the specific areas identified in figure 1: a) Si grain b) SiC grain

**Figure 3.** Mass variations ( $m-m_0$ ) according to the time, for the three samples oxidized in the conditions reported in table 1.

**Figure 4.** SEM images (x 1,000) of the oxidized Si-SiC samples a)  $t = 4 \times 20 \text{ min}$ ,  $T = 1470 \text{ K}$  b)  $t = 4 \times 20 \text{ min}$ ,  $T = 1530 \text{ K}$  c)  $t = 4 \times 60 \text{ min}$ ,  $T = 1500 \text{ K}$

**Figure 5.** EDS spectrum corresponding to the scanned surfaces presented in figure 4 a)  $t = 4 \times 20 \text{ min}$ ,  $T = 1470 \text{ K}$  b)  $t = 4 \times 20 \text{ min}$ ,  $T = 1530 \text{ K}$  c)  $t = 4 \times 60 \text{ min}$ ,  $T = 1500 \text{ K}$

**Figure 6.** Arithmetic ( $S_a = \overline{\Delta z}$ ), quadratic ( $S_q = \sqrt{\overline{\Delta z^2}}$ ) and maximal ( $S_z = z_{\max} - z_{\min}$ ) surface roughnesses of the Si-SiC samples before and after oxidation

**Figure 7.** Variation of the square of the mass variation with time (a) and dependence of the semi-parabolic constant  $k_p$  with the reverse temperature (b).

**Figure 8.** Refractive index (a) and extinction coefficient (b) as function of incident photon energy for reference (▪) and treated samples.  $\text{SiO}_2$  indexes are plotted for comparison.

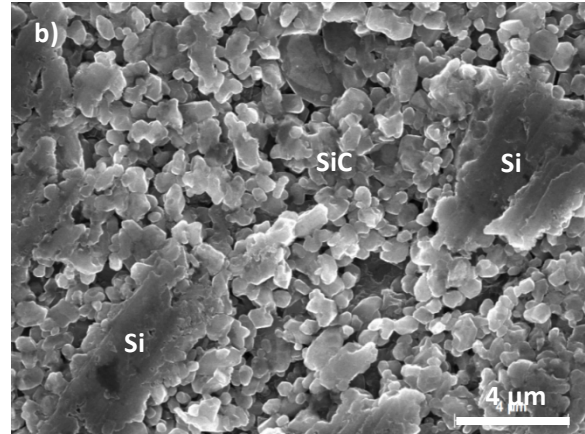
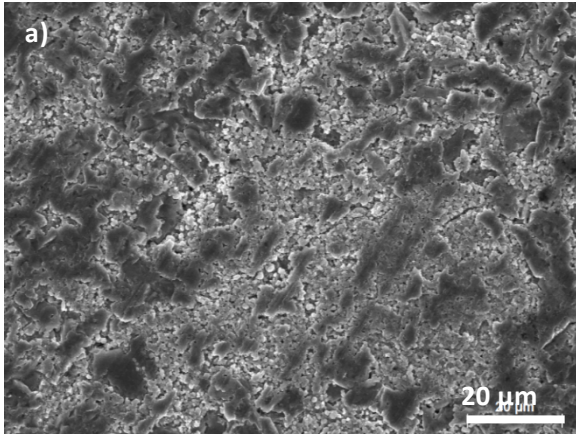
**Figure 9.** Cross-section SEM images and EDS cartography of O, Si and Al elements in the section of reference and oxidized Si-SiC samples.

**Figure 10.** Room temperature spectral emissivities measured in the  $0.25 - 2.5 \mu\text{m}$  (a) and  $2 - 25 \mu\text{m}$  (b) ranges, calculated solar absorptivity  $\alpha$  and total emissivity  $\varepsilon$  (c) and evolution of the  $\alpha/\varepsilon$  ratio (d), for reference and oxidized samples.

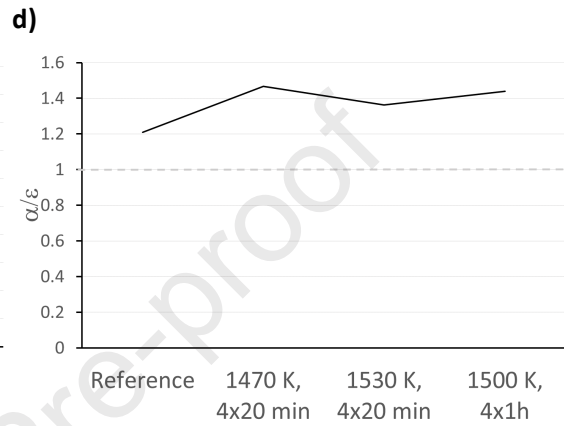
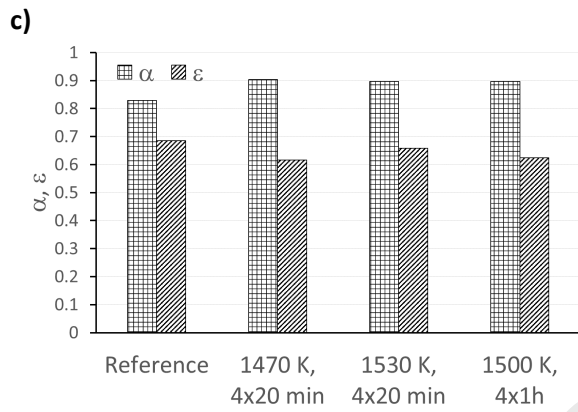
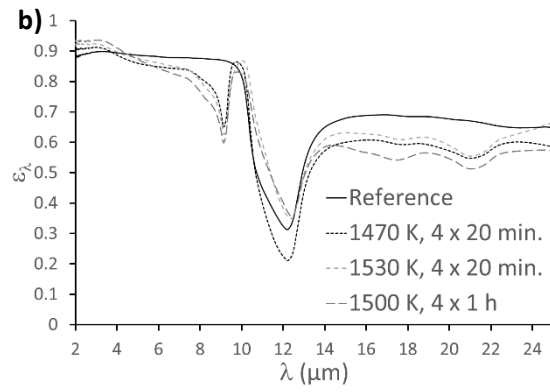
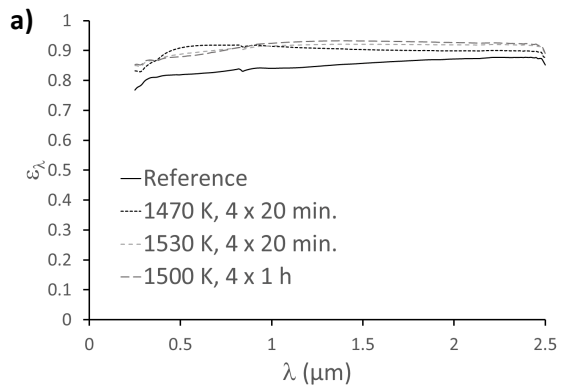
**Figure 11.** High temperature spectral emissivities measured in MEDIASE at three different temperatures of the Si-SiC sample oxidized during  $4 \times 1 \text{ h}$  at  $1500 \text{ K}$  (a) and evolution of the integrated  $\varepsilon_{1.4-2.8}$ ,  $\varepsilon_{1.4-14}$  and of their ratio (b) with T

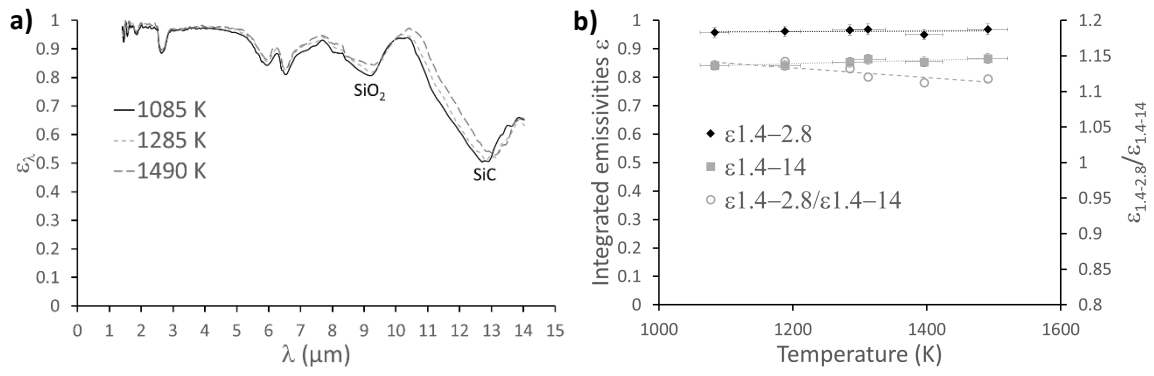
**Figure 12.** Thermal efficiency  $\eta_R$  of a Si-SiC solar receiver, non-oxidized and oxidized, according to its surface temperature  $T_w$ .

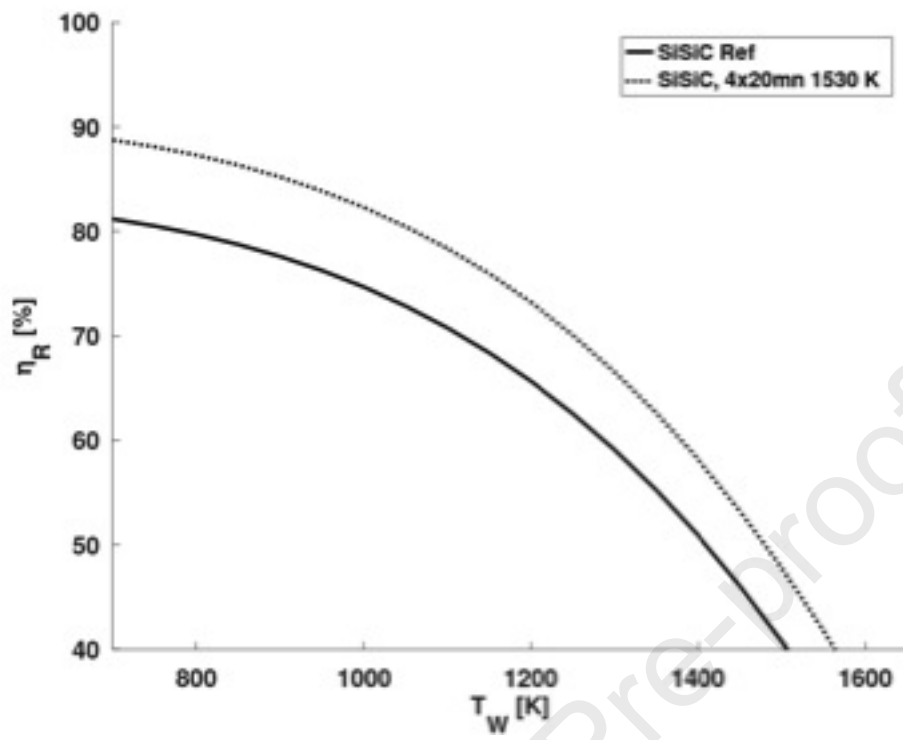
Journal Pre-proof



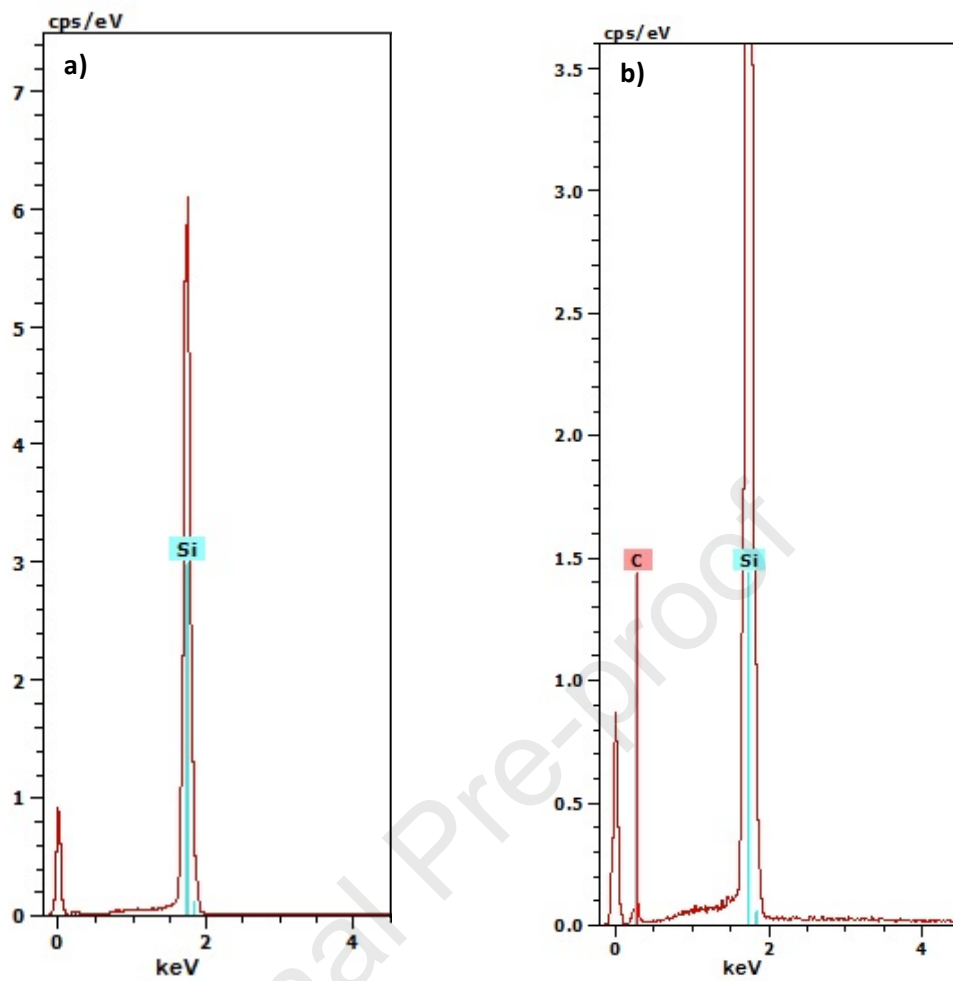
Journal Pre-proof

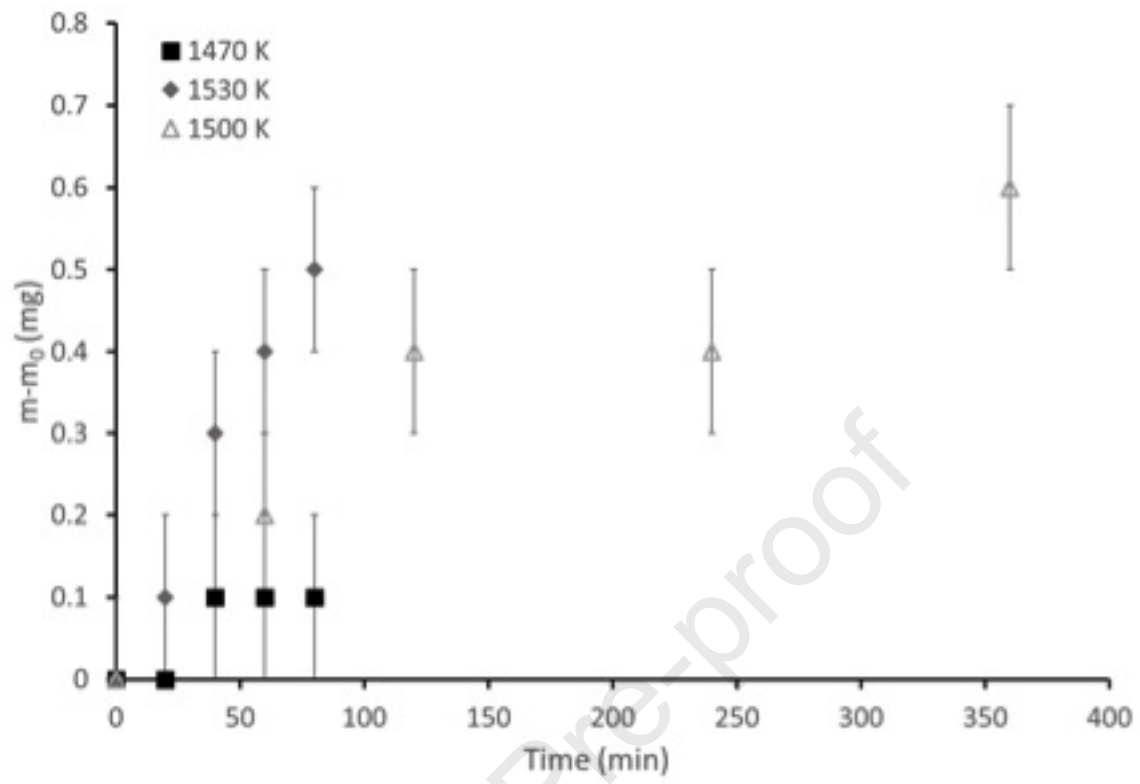


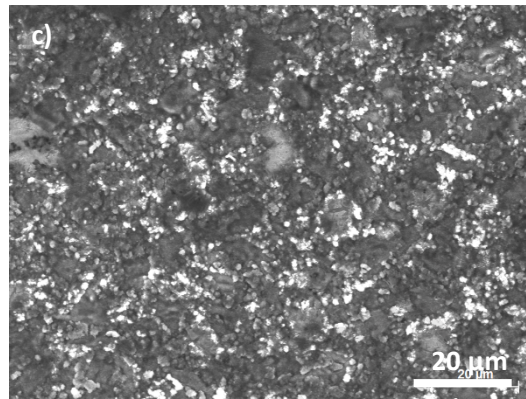
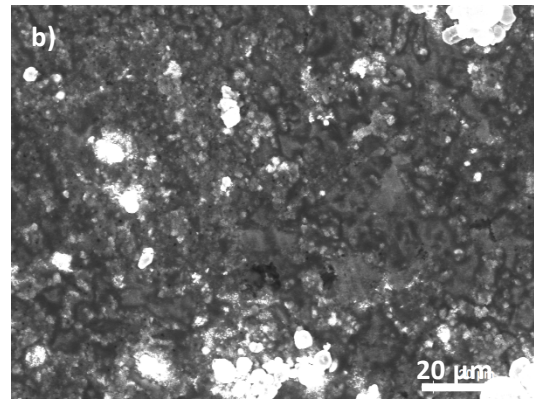
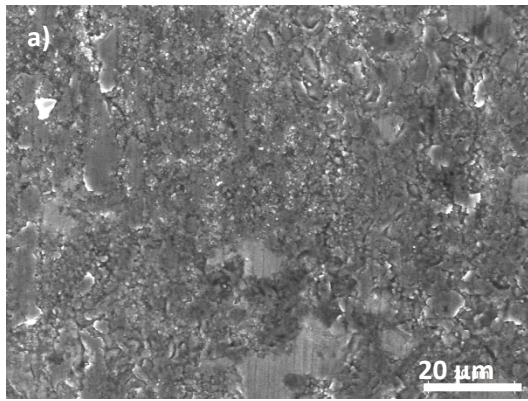


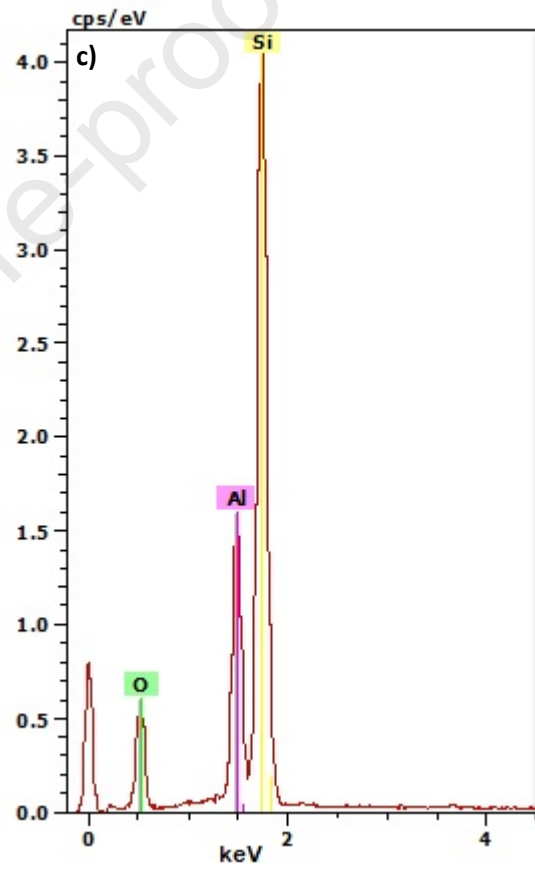
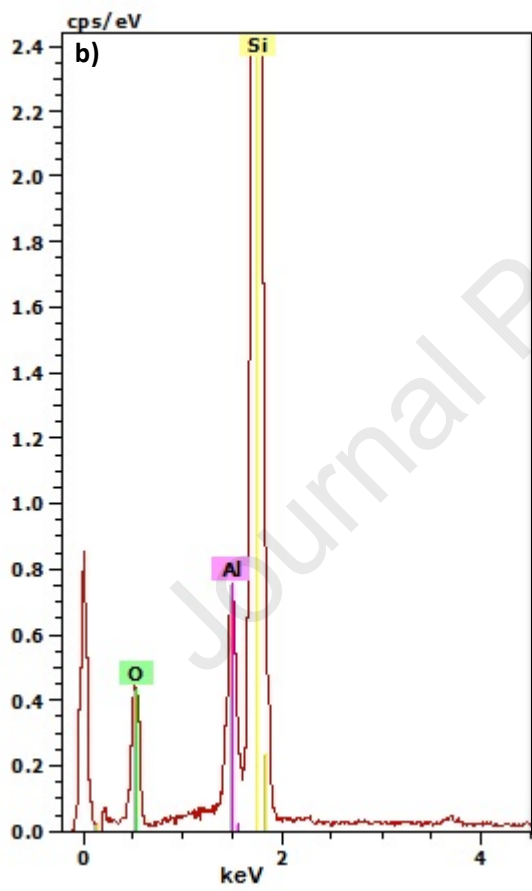
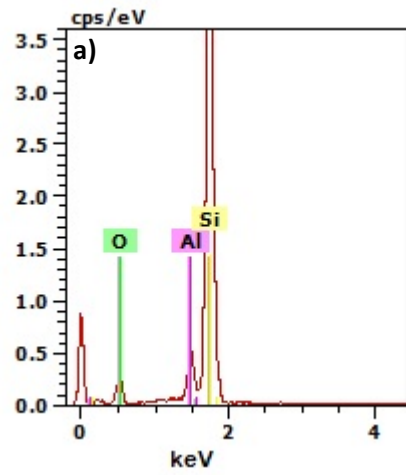


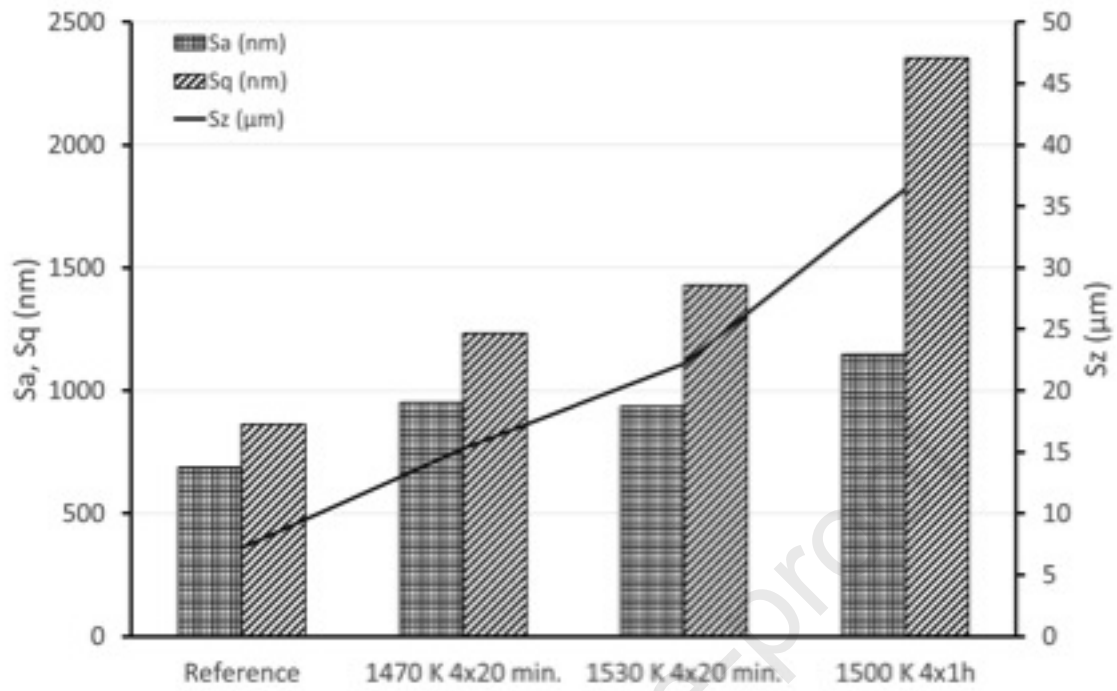


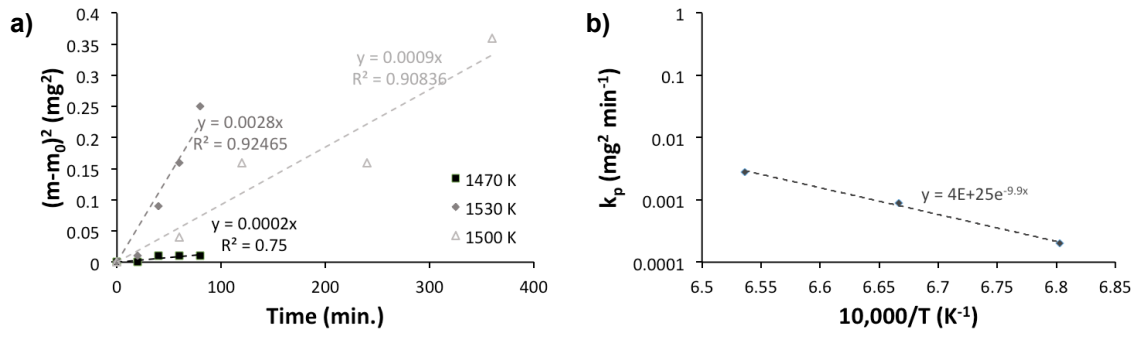


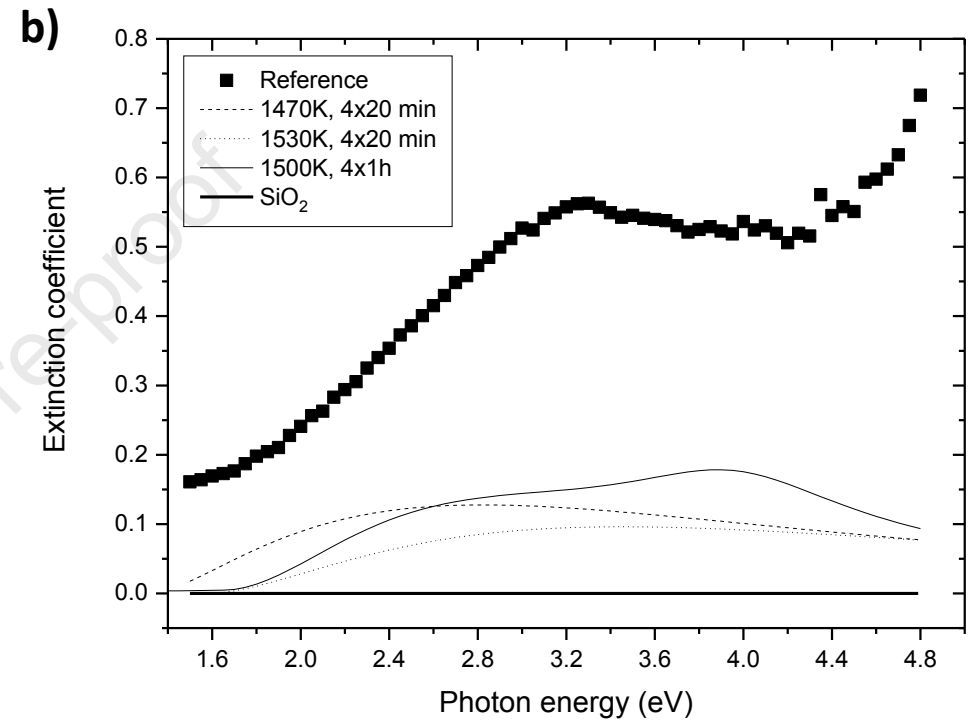
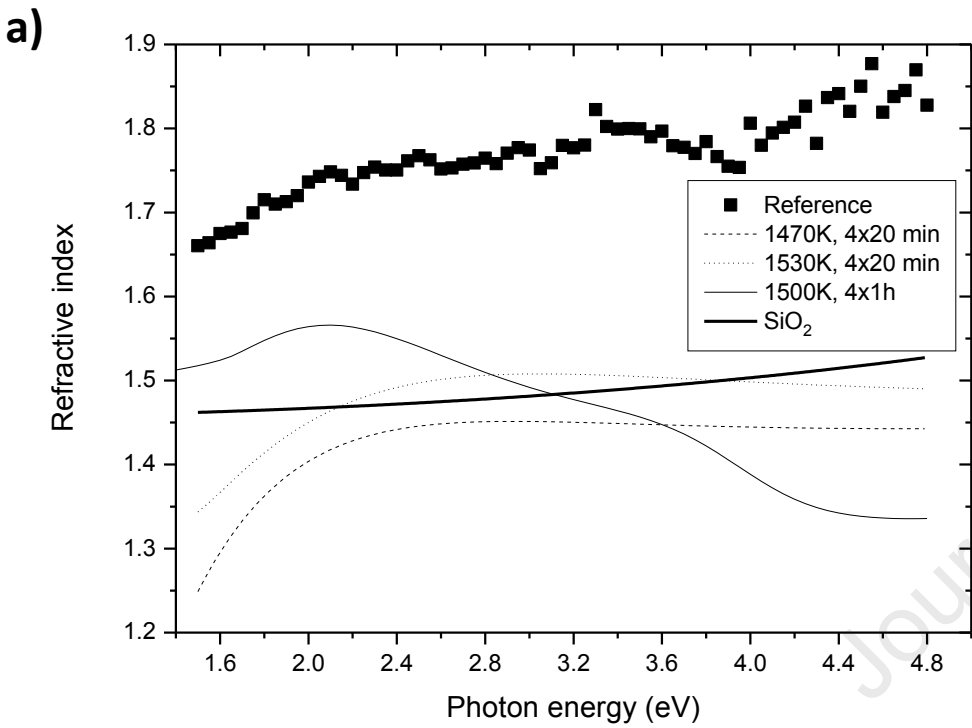


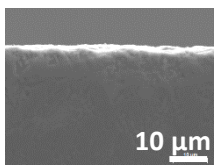
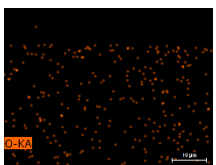
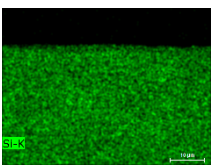
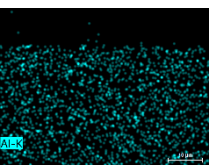
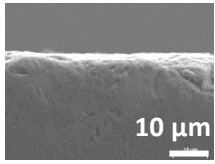
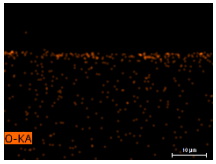
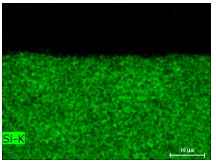
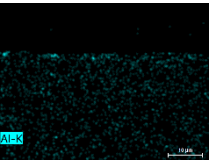
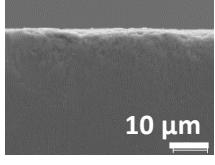
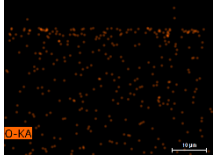
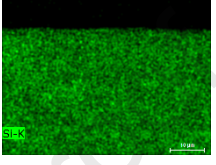
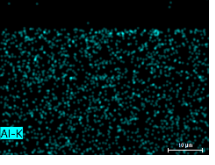
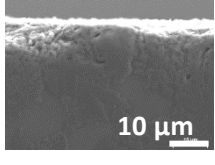
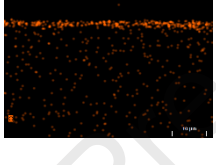
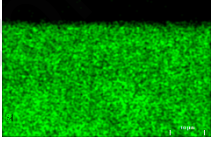
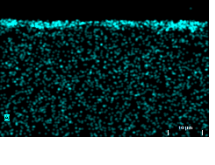










	SEM	EDS, O	EDS, Si	EDS, Al
Reference				
Si-SiC 4, 1470 K, 4x20 min.				
Si-SiC 5, 1530 K, 4x20 min.				
Si-SiC 6, 1500 K, 4x1h				



**Declaration of interests**

The authors declare that they have no known competing financial interests or personal relationships that could have appeared to influence the work reported in this paper.

The authors declare the following financial interests/personal relationships which may be considered as potential competing interests:

Journal Pre-proof